INTERNATIONAL JOURNAL FOR NUMERICAL METHODS IN FLUIDS
Int. J. Numer. Meth. Fluids 2008; **57**:1397–1420
Published online 28 April 2008 in Wiley InterScience (www.interscience.wiley.com). DOI: 10.1002/fld.1818

Adaptive finite element approximation of coupled flow and transport problems with applications in heat transfer

Mats G. Larson*,†,‡, Robert Söderlund§ and Fredrik Bengzon§

Department of Mathematics, Umeå University, S-90187 Umeå, Sweden

SUMMARY

In this paper we develop an adaptive finite element method for heat transfer in incompressible fluid flow. The adaptive method is based on an *a posteriori* error estimate for the coupled problem, which identifies how accurately the flow and heat transfer problems must be solved in order to achieve overall accuracy in a specified goal quantity. The *a posteriori* error estimate is derived using duality techniques and is of dual weighted residual type. We consider, in particular, an *a posteriori* error estimate for a variational approximation of the integrated heat flux through the boundary of a hot object immersed into a cooling fluid flow. We illustrate the method on some test cases involving three-dimensional time-dependent flow and transport. Copyright © 2008 John Wiley & Sons, Ltd.

Received 24 September 2007; Revised 21 February 2008; Accepted 5 March 2008

KEY WORDS: finite element methods; Navier–Stokes; adaptivity; error estimation; mesh adaptation; advection–diffusion equation

1. INTRODUCTION

Coupled multiphysics models appear in many real-world applications that involve several different types of physics that interact in space and time. Such problems are often solved numerically by connecting individual single physics solvers that handle each physics involved in the problem. It is then important to derive an efficient error estimation procedure that targets a specified goal quantity in the overall multiphysics problem and, in particular, identifies the influence of errors in the single physics solvers on the overall goal. On the basis of such error estimates we can develop adaptive algorithms that automatically determine a local mesh resolution for the individual solvers

*Correspondence to: Mats G. Larson, Department of Mathematics, Umeå University, S-90187 Umeå, Sweden.
†E-mail: mats.larson@math.umu.se
‡Professor of Applied Mathematics.
§Research Assistant.

tailored for efficient computation of the specified overall goal quantity. In this work we take a step in this direction and consider a model problem involving coupled time-dependent heat transfer and incompressible fluid flow, a common multiphysics problem in engineering applications.

Recently, there has been an increasing research interest in adaptive methods for multiphysics problems. A general framework for adaptive multiphysics solvers is presented in [1], where an application to microelectromechanical systems involving electrostatics, heat conduction, and elasticity is presented. In [2] pressure-driven transport is studied using a mixed method for the stationary pressure equation and a streamline diffusion method for the transport equation. Furthermore, recent closely related work is presented in [3, 4], where one-way-coupled and fully coupled elliptic systems are considered. We also mention *a posteriori* error estimates for operator splitting methods [5].

In this paper we start from the approach developed in [1], and derive an *a posteriori* error estimate for the coupled problem involving time-dependent incompressible flow governed by the Navier–Stokes equations and heat transfer with the advection field given by the fluid velocity. We restrict our attention to the one-way-coupled case where the fluid flow is independent of the temperature. Given a goal functional on the temperature field in the transport equation, our approach identifies a corresponding goal functional for the incompressible flow solver, which defines in what sense the flow field must be accurate in order to achieve accuracy in the given transport goal functional. The *a posteriori* error estimates are derived using duality-based techniques and result in dual weighted residual estimates with weights accounting for the specified goal functional and the coupling between the problems. We refer to [6, 7] for the duality-based *a posteriori* error analysis on incompressible flow problems and to [8–10], and the references therein for a more general background on duality-based techniques. Based on the *a posteriori* error estimates we develop adaptive algorithms for adaptive mesh refinement [11].

We study, in particular, a specific goal functional representing the total heat flux through the boundary of a hot object immersed into a cooling fluid flow. Here we make a particular use of a variational formulation of the flux functional, which plays an important role when computing the functional as well as for the derivation of the *a posteriori* error estimate, see [12–15].

Finally, the methodology is illustrated on a three-dimensional test case involving a number of hot boxes immersed into a channel containing a cooling fluid flow.

The outline of this paper is as follows: In Section 2 we present the model problem and the finite element methods; in Section 3 we derive the *a posteriori* error estimates, study the integrated flux functional, and formulate adaptive algorithms; in Section 4 we present the numerical examples; and, finally, in Section 5 we make some concluding remarks.

2. MODEL PROBLEM AND FINITE ELEMENT METHOD

2.1. Model problem

As a simple model problem we consider the transport of heat from a number of hot objects by a cooling fluid. The hot objects are one or two boxes located within a long channel with a square cross section. The fluid is flowing through the channel from an inlet to an outlet located on the short sides of the channel, see Figure 1. The boxes are kept at a prescribed temperature and heat is diffused and advected away from these by the surrounding fluid, which is assumed to have a lower temperature at the inflow, thereby acting as a coolant on and around the boxes.

DOI: 10.1002/fld

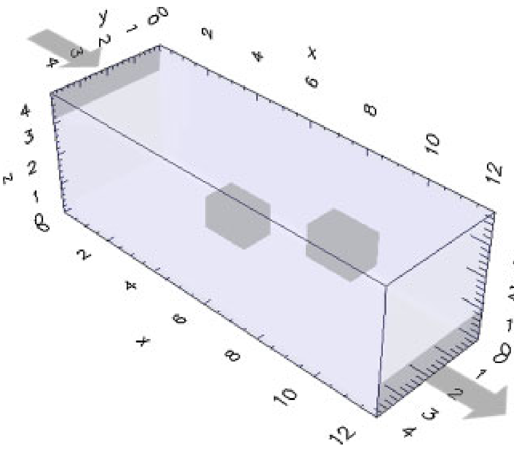

Figure 1. The channel geometry with two interior hot boxes. A cooling fluid is flowing through the channel. Inlet and outlet are the shaded regions indicated by the arrows.

To describe the geometry of this problem we employ the following notation. The channel domain is denoted by $\Omega\subset\mathbf{R}^3$, and its boundary $\partial\Omega$ by Γ. The inflow and outflow parts of Γ are denoted by Γ_{in} and Γ_{out}, and the walls of the channel by Γ_{wall}. Further, the sides of the hot boxes lying within the channel are denoted by Γ_{box}. Thus, $\Gamma=\Gamma_{\text{in}}\cup\Gamma_{\text{wall}}\cup\Gamma_{\text{out}}\cup\Gamma_{\text{box}}$. Finally, the outward unit normal of Γ is denoted by $\mathbf{n}$. Throughout this paper we shall let boldface letters denote vector-valued quantities. For example, the usual position vector $(x,y,z)\in\mathbf{R}^3$ is denoted by $\mathbf{x}$.

In this paper we make the simplifying assumption that any buoyancy forces within the fluid are negligible, which means that the tendency for heavy (cool) fluid to sink is very small (cf. [16]). As a consequence the fluid velocity, $\mathbf{u}_{\text{F}}$, is unaffected by the transport of heat within the fluid, and no new flow phenomena arise due to changes in the temperature of the fluid. In other words, we end up with a *one-way* coupled problem in the sense that the fluid temperature, u_{T}, depends on the fluid velocity $\mathbf{u}_{\text{F}}$, but not *vice versa*.

From a numerical point of view this one-way coupling implies that any errors present in an approximation, $\mathbf{U}_{\text{F}}$, of the velocity $\mathbf{u}_{\text{F}}$ will contribute to the error in a computation of the temperature if $\mathbf{U}_{\text{F}}$ is used as an advection field. Thus, a computed temperature $U_{\text{T}}\approx u_{\text{T}}$ will generally contain both a discretization error stemming from the numerical method and a data error caused by the inaccurate advection field $\mathbf{U}_{\text{F}}$. We will refer to this data error as the *modelling error* since it appears due to the inaccurate specification of the input to the heat equation. We aim at controlling the propagation of error from $\mathbf{U}_{\text{F}}$ to U_{T}.

We shall present a methodology for estimating the error in a given target quantity, defined by a linear functional $m_{\text{T}}(u_{\text{T}})$ of the temperature u_{T}. The functional $m_{\text{T}}(\cdot)$ expresses the overall goal of the computation, which can be the accurate computation of u_{T} at a point $\mathbf{a}\in\Omega$ or the mean value of u_{T} in a subdomain $\omega\in\Omega$, for instance. In Section 4 we shall let $m_{\text{T}}(\cdot)$ be the time-integrated heat flux out of one of the hot boxes, but we perform the analysis for an arbitrary goal functional $m_{\text{T}}(u_{\text{T}})$.

Our methodology consists of a standard *a posteriori* error estimation based on duality arguments (see, e.g. [8, 9] for overviews of these techniques). The basic idea is to transform the modelling error for the heat transfer problem into a discretization error for the fluid flow problem via a

DOI: 10.1002/fld

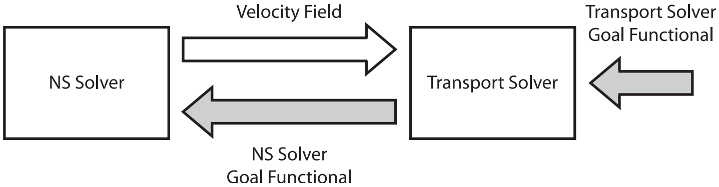

Figure 2. Schematic picture illustrating how to determine the target quantity $m_{\mathrm{T}}(u_{\mathrm{T}})$. The flow of primal data (i.e. the advection field $\mathbf{u}_{\mathrm{F}}$) is indicated by the white arrow and the dual data flow by the shaded arrows.

particular choice of the dual problem. We summarize the methodology as follows:

1. Start by computing the fluid velocity $\mathbf{U}_{\mathrm{F}}$. Use $\mathbf{U}_{\mathrm{F}}$ to compute the fluid temperature U_{T}.
2. Solve a dual heat problem associated with the given goal functional $m_{\mathrm{T}}(\cdot)$ for the dual temperature ϕ_{T}. A straightforward calculation shows that the error in $m_{\mathrm{T}}(\cdot)$ (i.e. $m_{\mathrm{T}}(u_{\mathrm{T}}-U_{\mathrm{T}})$) consists of a discretization error for U_{T} and a modelling error $m_{\mathrm{F}}(\cdot)$ involving the velocity error $\mathbf{u}_{\mathrm{F}}-\mathbf{U}_{\mathrm{F}}$.
3. To keep the modelling error small, let $m_{\mathrm{F}}(\cdot)$ be the goal functional for the fluid flow problem and solve an associated dual flow problem for the dual fluid velocity $\boldsymbol{\phi}_{\mathrm{F}}$.
4. The dual information ϕ_{T} and $\boldsymbol{\phi}_{\mathrm{F}}$ indicate the domain of influence for the functionals $m_{\mathrm{T}}(\cdot)$ and $m_{\mathrm{F}}(\cdot)$, that is, regions of Ω where it is important to compute the fluid velocity $\mathbf{U}_{\mathrm{F}}$ and temperature U_{T} accurately. The key point is that by choosing $m_{\mathrm{F}}(\cdot)$ as the goal for the fluid flow problem the modelling error of the previous heat transfer problem transforms into a discretization error for $\mathbf{U}_{\mathrm{F}}$. Moreover, since we assume input to be exact for the fluid flow problem the only source of error for $\mathbf{U}_{\mathrm{F}}$ is the discretization error. Thus, we end up with two discretization errors, one for U_{T} and one for $\mathbf{U}_{\mathrm{F}}$, which can be kept small via standard *a posteriori* estimates together with the adaptive mesh refinement.
5. The procedure is repeated until a mesh yielding a sufficiently accurate value of $m_{\mathrm{T}}(\cdot)$ has been obtained.

In Figure 2 we illustrate the procedure for estimating $m_{\mathrm{T}}(u_{\mathrm{T}}-U_{\mathrm{T}})$ described above.

Finally, we wish to stress the fact that the main objective of this paper is not to provide numerical results for a specific physical application, but to present a method for efficient computation of a given goal quantity.

2.1.1. Governing equations. The motion of the fluid is governed by the incompressible Navier–Stokes equations that take the form: find the velocity $\mathbf{u}_{\mathrm{F}}=\mathbf{u}_{\mathrm{F}}(\mathbf{x},t):\Omega\times I\rightarrow\mathbf{R}^3$ and the pressure $p=p(\mathbf{x},t):\Omega\times I\rightarrow\mathbf{R}$ such that

$$\dot{\mathbf{u}}_{\mathrm{F}}+\mathbf{u}_{\mathrm{F}}\cdot\nabla\mathbf{u}_{\mathrm{F}}-\nu\Delta\mathbf{u}_{\mathrm{F}}+\frac{1}{\rho}\nabla p=\mathbf{f},\quad(\mathbf{x},t)\in\Omega\times I \tag{1a}$$

$$\nabla\cdot\mathbf{u}_{\mathrm{F}}=0,\quad(\mathbf{x},t)\in\Omega\times I \tag{1b}$$

$$\mathbf{u}_{\mathrm{F}}=\mathbf{v}_{\mathrm{in}},\quad(\mathbf{x},t)\in\Gamma_{\mathrm{in}}\times I \tag{1c}$$

$$\mathbf{u}_{\mathrm{F}}=\mathbf{0},\quad(\mathbf{x},t)\in\Gamma_{\mathrm{wall}}\cup\Gamma_{\mathrm{box}}\times I \tag{1d}$$

DOI: 10.1002/fld

$$\nu\mathbf{n}\cdot\nabla\mathbf{u}_{\mathrm{F}}-\frac{1}{\rho}p\mathbf{n}=0, \quad (\mathbf{x},t)\in\Gamma_{\mathrm{out}}\times I \tag{1e}$$

$$\mathbf{u}_{\mathrm{F}}(\cdot,0)=0, \quad \mathbf{x}\in\Omega \tag{1f}$$

where ν is the kinematic viscosity, ρ is the (constant) density of the fluid, and $\mathbf{f}=\mathbf{0}$ is a body force term, which is zero due to the absence of buoyancy forces (cf. Remark 2.1). Further, $\dot{\mathbf{u}}_{\mathrm{F}}$ is the derivative $\partial\mathbf{u}_{\mathrm{F}}/\partial t$ with respect to time t and $I=(0,\hat{T})$ is the time interval with final time $\hat{T}$. A given velocity profile $\mathbf{v}_{\mathrm{in}}$ is prescribed on the inflow, and on the outflow we use the 'do nothing' boundary condition (1e) (see [17]). All the other boundaries have no-slip boundary conditions.

The equation for the heat transfer takes the form: find the temperature $u_{\mathrm{T}}=u_{\mathrm{T}}(\mathbf{x},t):\Omega\times I\rightarrow\mathbf{R}$ such that

$$\dot{u}_{\mathrm{T}}+\nabla\cdot(\mathbf{u}_{\mathrm{F}}u_{\mathrm{T}}-\varepsilon\nabla u_{\mathrm{T}})=0, \quad (\mathbf{x},t)\in\Omega\times I \tag{2a}$$

$$\mathbf{n}\cdot(\mathbf{u}_{\mathrm{F}}u_{\mathrm{T}}-\varepsilon\nabla u_{\mathrm{T}})=\kappa(u_{\mathrm{T}}-g), \quad (\mathbf{x},t)\in\Gamma\times I \tag{2b}$$

$$u_{\mathrm{T}}(\cdot,0)=0, \quad \mathbf{x}\in\Omega \tag{2c}$$

where $\mathbf{u}_{\mathrm{F}}$ is the advection field induced by the Navier–Stokes equations (1), ε is the thermal diffusion parameter of the fluid, κ is a given function describing the heat transfer coefficient to the ambient media, and g is the temperature of the ambient media.

Remark 2.1

Temperature effects on the fluid velocity can under certain assumptions be modelled by the Boussinesque approximation in which a buoyancy force term of the form $\mathbf{f}=-\gamma\mathbf{g}(u_{\mathrm{T}}-u_{\infty})$ is added to the momentum equation (1a) with u_{∞} being a reference temperature, γ the thermal expansion coefficient of the fluid, and $\mathbf{g}=[0,0,-1]^{\mathrm{T}}$ (cf. [18]). However, note that the addition of a buoyancy force yields a more intricate two-way coupling between (1) and (2) since $\mathbf{u}_{\mathrm{F}}$ in this case will depend on u_{T} and *vice versa*. We refer to [19] for a discussion of error estimation techniques for fully coupled problems.

2.2. Variational formulations

Before we proceed any further let us introduce some notations that will be of frequent use. We let

$$(\mathbf{v},\mathbf{w})_{\omega}=\int_{\omega}\mathbf{v}\cdot\mathbf{w}\,\mathrm{d}\mathbf{x} \tag{3}$$

denote the L^2 inner product on the set ω. When $\omega=\Omega$ we shall for brevity write $(\cdot,\cdot)=(\cdot,\cdot)_{\Omega}$. The L^2 norm of $\mathbf{v}$ on ω is denoted by $\|\mathbf{v}\|_{\omega}=\sqrt{(\mathbf{v},\mathbf{v})_{\omega}}$. In order to state the variational formulation of (1) and (2) we need to define the appropriate function spaces for the velocity pressure pair ($\mathbf{u}_{\mathrm{F}}$, p) and the temperature u_{T}. Therefore, let $\mathbf{H}_0^1(\Omega)=\{\mathbf{v}\in[H^1(\Omega)]^3:\mathbf{v}|_{\Gamma\backslash\Gamma_{\mathrm{out}}}=\mathbf{0}\}$, and

$$\mathbf{V}_{\mathrm{F}}=L^2(I;\mathbf{H}_0^1(\Omega)\times L^2(\Omega)) \tag{4}$$

$$V_{\mathrm{T}}=L^2(I;H^1(\Omega)) \tag{5}$$

where $L^2(I;X)$ is the space of functions $v:I\rightarrow X$ such that $\int_I\|v(\cdot,t)\|_X^2\,\mathrm{d}t<\infty$, with X being a normed vector space.

DOI: 10.1002/fld

Let $\mathbf{u}_{\text{in}} \in \mathbf{H}_0^1(\Omega)$ be a suitable extension of the inflow velocity profile $\mathbf{v}_{\text{in}}$ to the whole domain Ω. The variational formulation of the Navier–Stokes equations (1) reads: find $(\mathbf{u}_{\text{F}}, p) \in (\mathbf{u}_{\text{in}}, 0) + \mathbf{V}_{\text{F}}$ such that

$$a_{\text{F}}((\mathbf{u}_{\text{F}}, p), (\mathbf{v}, q)) = 0 \quad \forall (\mathbf{v}, q) \in \mathbf{V}_{\text{F}} \tag{6}$$

where the space–time nonlinear form $a_{\text{F}}(\cdot, \cdot)$ is defined by

$$a_{\text{F}}((\mathbf{u}_{\text{F}}, p), (\mathbf{v}, q)) = \int_I (\dot{\mathbf{u}}_{\text{F}}, \mathbf{v}) + (\mathbf{u}_{\text{F}} \cdot \nabla \mathbf{u}_{\text{F}}, \mathbf{v}) + \nu(\nabla \mathbf{u}_{\text{F}}, \nabla \mathbf{v}) - \frac{1}{\rho}(p, \nabla \cdot \mathbf{v}) - (\nabla \cdot \mathbf{u}_{\text{F}}, q)\, \mathrm{d}t \tag{7}$$

For the heat transfer problem (2) the variational formulation reads: find $u_{\text{T}} \in V_{\text{T}}$, such that

$$a_{\text{T}}(\mathbf{u}_{\text{F}}; u_{\text{T}}, w) = l_{\text{T}}(w) \quad \forall w \in V_{\text{T}} \tag{8}$$

where the bilinear and linear forms $a_{\text{T}}(\cdot, \cdot)$ and $l_{\text{T}}(\cdot)$ are defined by

$$a_{\text{T}}(\mathbf{u}_{\text{F}}; u_{\text{T}}, w) = \int_I (\dot{u}_{\text{T}}, w) - (\mathbf{u}_{\text{F}} u_{\text{T}}, \nabla w) + (\varepsilon \nabla u_{\text{T}}, \nabla w) + (\kappa u_{\text{T}}, w)_\Gamma \, \mathrm{d}t \tag{9a}$$

$$l_{\text{T}}(w) = \int_I (\kappa g, w)_\Gamma \, \mathrm{d}t \tag{9b}$$

Combining the variational form for the Navier–Stokes and heat transfer equations we obtain the coupled problem: find $(\mathbf{u}_{\text{F}}, p) \in (\mathbf{u}_{\text{in}}, 0) + \mathbf{V}_{\text{F}}$ and $u_{\text{T}} \in V_{\text{T}}$ such that

$$a_{\text{F}}((\mathbf{u}_{\text{F}}, p), (\mathbf{v}, q)) = 0 \quad \forall (\mathbf{v}, q) \in \mathbf{V}_{\text{F}} \tag{10a}$$

$$a_{\text{T}}(\mathbf{u}_{\text{F}}; u_{\text{T}}, w) = l_{\text{T}}(w) \quad \forall w \in V_{\text{T}} \tag{10b}$$

2.3. Discrete spaces

Let $\mathscr{K}$ a be a shape regular [20] mesh of Ω consisting of hexahedra or tetrahedra K with diameter $h_K = \text{diam}(K)$, and let $V_h \subset H^1(\Omega)$, $\mathbf{V}_h \subset \mathbf{H}_0^1(\Omega)$, and $Q_h \subset L^2(\Omega)$, be three spaces of continuous piecewise polynomials on $\mathscr{K}$. Further, let $0 = t_0 < t_1 < \cdots < t_N = \hat{T}$ be a partition of the time interval I into N subintervals $I_n = (t_{n-1}, t_n]$, $n = 1, \ldots, N$, of length $k_n = t_n - t_{n-1}$.

On each space–time slab $S_n = \Omega \times I_n$ we define the following function spaces that we shall use as trial and test spaces for the finite element method to be introduced next:

$$\mathbf{V}_n^q = \{(\mathbf{v}, w) : (\mathbf{v}, w)(\cdot, t) \in \mathbf{V}_h \times Q_h, (\mathbf{v}, w)(\mathbf{x}, \cdot) \in \mathscr{P}_q \times \mathscr{P}_q\} \tag{11}$$

$$\mathbf{W}_n = \mathbf{V}_n^0 \tag{12}$$

$$V_n^q = \{v : v(\cdot, t) \in V_h, v(\mathbf{x}, \cdot) \in \mathscr{P}_q\} \tag{13}$$

$$W_n = V_n^0 \tag{14}$$

where $\mathscr{P}_q$ is the space of polynomials of degree not exceeding q on I_n. The corresponding 'global' spaces on $\Omega\times I$ are given by

$$\mathbf{V}_{\mathrm{F},h,n}=\{(\mathbf{v},w):(\mathbf{v},w)|_{S_n}\in\mathbf{V}_n^1, n=1,\dots,N,\ \text{and } (\mathbf{v},w) \text{ continuous w.r.t. time}\} \tag{15}$$

$$\mathbf{W}_{\mathrm{F},h,n}=\{(\mathbf{v},w):(\mathbf{v},w)|_{S_n}\in\mathbf{W}_n, n=1,\dots,N\} \tag{16}$$

$$V_{\mathrm{T},h,n}=\{v:v|_{S_n}\in V_n^1, n=1,\dots,N,\ \text{and } v \text{ continuous w.r.t. time}\} \tag{17}$$

$$W_{\mathrm{T},h,n}=\{v:v|_{S_n}\in W_n, n=1,\dots,N\} \tag{18}$$

We also need to introduce two interpolation operators onto the discrete spaces. Let $\pi_{\mathrm{T}}:V_{\mathrm{T}}\rightarrow W_{\mathrm{T},h,n}$ be the interpolation operator obtained by combining the Scott–Zhang [21] interpolation operator with a projection operator onto the space of piecewise constants on the time partition $\{t_n\}_0^N$. That is, $\pi_{\mathrm{T}}v$ on the slab $S_n=\Omega\times I_n$ is the Scott–Zhang interpolant on V_h for $\mathbf{x}\in\Omega$ and the average of v on I_n for $t\in I_n$. Further, let $\pi_{\mathrm{F}}:\mathbf{V}_{\mathrm{F}}\rightarrow\mathbf{W}_{\mathrm{F},h,n}$ be the vector-valued analog to π_{T}. As it will always be clear from the context which interpolation operator we refer to, we will drop the subscripts on π_{T} and π_{F} and simply write π from now on.

2.4. *Finite element approximation*

A prototype finite element method for the coupled problem (10) takes the form: find $(\mathbf{U}_{\mathrm{F}},P)\in(\mathbf{u}_{\mathrm{in}},0)+\mathbf{V}_{\mathrm{F},h,n}$, and $U_{\mathrm{T}}\in V_{\mathrm{T},h,n}$ such that

$$a_{\mathrm{F}}((\mathbf{U}_{\mathrm{F}},P),(\mathbf{v},q))=0 \quad \forall(\mathbf{v},q)\in\mathbf{W}_{\mathrm{F},h,n} \tag{19a}$$

$$a_{\mathrm{T}}(\mathbf{U}_{\mathrm{F}};U_{\mathrm{T}},w)=l_{\mathrm{T}}(w) \quad \forall w\in W_{\mathrm{T},h,n} \tag{19b}$$

Remark 2.2

The finite element method (19) is a standard space–time Galerkin method for the coupled problem (10) and has to be modified for nearly all practical purposes to yield useful numerical results. For example, to obtain a unique solution it is necessary for the velocity and pressure spaces $\mathbf{V}_h$ and Q_h to satisfy the so-called inf–sup condition, cf. [20]. This generally excludes the use of equal-order interpolation spaces unless some stabilization term for the pressure is added to the incompressibility equation (1b). Stabilization terms (see, e.g. [22]) are also necessary for both the Navier–Stokes equations and the heat transport equation in order to make simulations of fluids with small viscosity v and thermal diffusion coefficient ε. We shall briefly return to these issues in the numerics section.

Remark 2.3

The reason why we formulate a prototype method is that we want to focus on the error analysis, which usually does not depend on the particular type of discretization to any large extent. For simplicity of presentation we therefore argue that it suffice to study (19). We stress that the error estimation technique we present may be employed for many different finite element methods with only minor modifications.

3. *A POSTERIORI* ERROR ESTIMATES

3.1. Error representation formula for the coupled problem

Let $m_\mathrm{T}(u_\mathrm{T})$ be a linear functional of the temperature $u_\mathrm{T} \in H^1(\Omega)$ expressing the goal of the computation. To derive an error representation formula for $m_\mathrm{T}(\cdot)$ we introduce the following dual heat transfer problem: find $\phi_\mathrm{T} \in V_\mathrm{T}$ such that

$$m_\mathrm{T}(v) = a_\mathrm{T}(\mathbf{U}_\mathrm{F}; v, \phi_\mathrm{T}) \quad \forall v \in V_\mathrm{T} \tag{20}$$

Setting $v = u_\mathrm{T} - U_\mathrm{T}$ and using the definition of the dual problem (20) we obtain

$$\begin{aligned} m_\mathrm{T}(u_\mathrm{T} - U_\mathrm{T}) &= a_\mathrm{T}(\mathbf{U}_\mathrm{F}; u_\mathrm{T} - U_\mathrm{T}, \phi_\mathrm{T}) & (21)\\ &= a_\mathrm{T}(\mathbf{U}_\mathrm{F}; u_\mathrm{T}, \phi_\mathrm{T}) - a_\mathrm{T}(\mathbf{U}_\mathrm{F}; U_\mathrm{T}, \phi_\mathrm{T}) & (22)\\ &= a_\mathrm{T}(\mathbf{U}_\mathrm{F}; u_\mathrm{T}, \phi_\mathrm{T}) - a_\mathrm{T}(\mathbf{u}_\mathrm{F}; u_\mathrm{T}, \phi_\mathrm{T})\\ &\quad + a_\mathrm{T}(\mathbf{u}_\mathrm{F}; u_\mathrm{T}, \phi_\mathrm{T}) - a_\mathrm{T}(\mathbf{U}_\mathrm{F}; U_\mathrm{T}, \phi_\mathrm{T}) & (23)\\ &= a_\mathrm{T}(\mathbf{U}_\mathrm{F}; u_\mathrm{T}, \phi_\mathrm{T}) - a_\mathrm{T}(\mathbf{u}_\mathrm{F}; u_\mathrm{T}, \phi_\mathrm{T})\\ &\quad + l_\mathrm{T}(\phi_\mathrm{T}) - a_\mathrm{T}(\mathbf{U}_\mathrm{F}; U_\mathrm{T}, \phi_\mathrm{T}) & (24)\\ &= a_\mathrm{T}(\mathbf{U}_\mathrm{F}; u_\mathrm{T}, \phi_\mathrm{T}) - a_\mathrm{T}(\mathbf{u}_\mathrm{F}; u_\mathrm{T}, \phi_\mathrm{T})\\ &\quad + l_\mathrm{T}(\phi_\mathrm{T} - \pi\phi_\mathrm{T}) - a_\mathrm{T}(\mathbf{U}_\mathrm{F}; U_\mathrm{T}, \phi_\mathrm{T} - \pi\phi_\mathrm{T}) & (25) \end{aligned}$$

where we have used the Galerkin orthogonality property to subtract an interpolant $\pi\phi_\mathrm{T} \in W_{\mathrm{T},h,n}$.

Defining the weak residual $R_\mathrm{T}(U_\mathrm{T}) \in V_\mathrm{T}^*$, where V_T^* is the dual of V_T, by

$$\langle R_\mathrm{T}(U_\mathrm{T}), v\rangle_{\Omega\times I} = l_\mathrm{T}(v) - a_\mathrm{T}(\mathbf{U}_\mathrm{F}; U_\mathrm{T}, v) \quad \forall v \in V_\mathrm{T} \tag{26}$$

where $\langle\cdot,\cdot\rangle$ denotes the duality pairing between V_T and V_T^*, and introducing the functional $m_\mathrm{F}(\cdot)$ defined by

$$m_\mathrm{F}(\mathbf{u}_\mathrm{F} - \mathbf{U}_\mathrm{F}) = a_\mathrm{T}(\mathbf{U}_\mathrm{F}; u_\mathrm{T}, \phi_\mathrm{T}) - a_\mathrm{T}(\mathbf{u}_\mathrm{F}; u_\mathrm{T}, \phi_\mathrm{T}) \tag{27}$$

we obtain the error representation formula

$$m_\mathrm{T}(u_\mathrm{T} - U_\mathrm{T}) = \langle R_\mathrm{T}(U_\mathrm{T}), \phi_\mathrm{T} - \pi\phi_\mathrm{T}\rangle_{\Omega\times I} + m_\mathrm{F}(\mathbf{u}_\mathrm{F} - \mathbf{U}_\mathrm{F}) \tag{28}$$

The first term on the right-hand side of (28) is the discretization error caused by the finite element approximation and the second term can be interpreted as a modelling error stemming from the approximate advection field $\mathbf{U}_\mathrm{F}$.

The discretization error may be estimated using the dual weighted residual method (see, e.g. [8]), and can be controlled using standard adaptive mesh refinement [11] techniques. The modelling error $m_\mathrm{F}(\mathbf{u}_\mathrm{F} - \mathbf{U}_\mathrm{F})$ accounts for the effects of errors within the computed flow field on the specified output functional $m_\mathrm{T}(\cdot)$. To estimate the modelling error functional $m_\mathrm{F}(\cdot)$ we are naturally led to deriving a duality-based *a posteriori* error estimate for the finite element approximation of the flow problem (1), with the modelling error as a goal quantity. In other words, the desired goal quantity

DOI: 10.1002/fld

for the flow problem (1) is the modelling error from the heat transfer problem (2). Note that the goal functional $m_{\mathrm{F}}(\cdot)$ appears naturally when applying the duality-based error estimation approach above on the heat equation and depends on the information from both the dual and primal heat transfer problems.

3.2. Estimates of the discretization error for the heat transfer

To estimate the discretization error we proceed as follows:

$$\begin{aligned}\langle R_{\mathrm{T}}(U_{\mathrm{T}}), \phi_{\mathrm{T}}-\pi\phi_{\mathrm{T}}\rangle_{\Omega\times I} &= l_{\mathrm{T}}(\phi_{\mathrm{T}}-\pi\phi_{\mathrm{T}})-a_{\mathrm{T}}(\mathbf{U}_{\mathrm{F}}; U_{\mathrm{T}}, \phi_{\mathrm{T}}-\pi\phi_{\mathrm{T}}) &(29)\\ &= \int_I (\kappa(g-U_{\mathrm{T}}), \phi_{\mathrm{T}}-\pi\phi_{\mathrm{T}})_\Gamma-(\dot{U}_{\mathrm{T}}, \phi_{\mathrm{T}}-\pi\phi_{\mathrm{T}})\\ &\quad -(\varepsilon\nabla U_{\mathrm{T}}, \nabla(\phi_{\mathrm{T}}-\pi\phi_{\mathrm{T}}))+(\mathbf{U}_{\mathrm{F}}U_{\mathrm{T}}, \nabla(\phi_{\mathrm{T}}-\pi\phi_{\mathrm{T}}))\,\mathrm{d}t &(30)\end{aligned}$$

Expressing this as a sum over the elements and using partial integration we obtain

$$\begin{aligned}\langle R_{\mathrm{T}}(U_{\mathrm{T}}), \phi_{\mathrm{T}}-\pi\phi_{\mathrm{T}}\rangle_{\Omega\times I} = \sum_{K\in\mathscr{K}}\int_I &-(\dot{U}_{\mathrm{T}}, \phi_{\mathrm{T}}-\pi\phi_{\mathrm{T}})_K\\ &+(\varepsilon\Delta U_{\mathrm{T}}, \phi_{\mathrm{T}}-\pi\phi_{\mathrm{T}})_K+\frac{1}{2}(\varepsilon[\mathbf{n}\cdot\nabla U_{\mathrm{T}}], \phi_{\mathrm{T}}-\pi\phi_{\mathrm{T}})_{\partial K\setminus\Gamma}\\ &-(\nabla\cdot(\mathbf{U}_{\mathrm{F}}U_{\mathrm{T}}), \phi_{\mathrm{T}}-\pi\phi_{\mathrm{T}})_K+(-\varepsilon\mathbf{n}\cdot\nabla U_{\mathrm{T}}+\mathbf{n}\cdot\mathbf{U}_{\mathrm{F}}U_{\mathrm{T}}\\ &+\kappa(g-U_{\mathrm{T}}), \phi_{\mathrm{T}}-\pi\phi_{\mathrm{T}})_{\partial K\cap\Gamma}\,\mathrm{d}t \qquad (31)\end{aligned}$$

The term $[\mathbf{n}\cdot\nabla U_{\mathrm{T}}]$ denotes the jump of the normal derivative of U_{T}, and appears since $\mathbf{n}\cdot\nabla U_{\mathrm{T}}$ is not continuous across the element boundaries. The terms on the boundary Γ account for the fact that the boundary conditions are only weakly enforced by the finite element method.

Noting that the residual on each element K consists of contributions from both the interior and the boundary ∂K of K, we introduce the following notation with cell and edge residuals:

$$R_{\mathrm{T},K} = \|-\dot{U}_{\mathrm{T}}-\nabla\cdot(\mathbf{U}_{\mathrm{F}}U_{\mathrm{T}})+\varepsilon\Delta U_{\mathrm{T}}\|_K \qquad (32)$$

$$r_{\mathrm{T},\partial K} = \tfrac{1}{2}\|\varepsilon[\mathbf{n}\cdot\nabla U_{\mathrm{T}}]\|_{\partial K\setminus\Gamma}+\|\mathbf{n}\cdot\mathbf{U}_{\mathrm{F}}U_{\mathrm{T}}-\varepsilon\mathbf{n}\cdot\nabla U_{\mathrm{T}}+\kappa(g-U_{\mathrm{T}})\|_{\partial K\cap\Gamma} \qquad (33)$$

Using the Cauchy–Schwartz inequality we can estimate the discretization error by

$$\langle R_{\mathrm{T}}(U_{\mathrm{T}}), \phi_{\mathrm{T}}-\pi\phi_{\mathrm{T}}\rangle_{\Omega\times I}\leqslant \sum_{K\in\mathscr{K}}\int_I (R_{\mathrm{T},K}\|\phi_{\mathrm{T}}-\pi\phi_{\mathrm{T}}\|_K+r_{\mathrm{T},\partial K}\|\phi_{\mathrm{T}}-\pi\phi_{\mathrm{T}}\|_{\partial K})\,\mathrm{d}t \qquad (34)$$

Moreover, using the trace inequality $\|v\|_{\partial K}\leqslant C(h_K^{-1/2}\|v\|_K+h_K^{1/2}\|\nabla v\|_K)$ (see [23]) and the interpolation estimate $\|\phi-\pi\phi\|_K\leqslant C(k_n\|\dot{\phi}\|_K+h_K\|\nabla\phi\|_K)$, $t\in I_n$ (see [21]), we can estimate (34) with

$$\langle R_{\mathrm{T}}(U_{\mathrm{T}}), \phi_{\mathrm{T}}-\pi\phi_{\mathrm{T}}\rangle_{\Omega\times I}\leqslant \sum_{K\in\mathscr{K}} \rho_{\mathrm{T},K}\,\omega_{\mathrm{T},K} \qquad (35)$$

where $\rho_{\mathrm{T},K}$ and $\omega_{\mathrm{T},K}$ are time-averaged element indicators given by

$$\rho_{\mathrm{T},K}=\int_I (R_{\mathrm{T},K}+h_K^{-1/2} r_{\mathrm{T},\partial K})\,\mathrm{d}t \tag{36}$$

$$\omega_{\mathrm{T},K}=C\int_I (k_n\|\dot{\phi}_\mathrm{T}\|_K+h_K\|\nabla\phi_\mathrm{T}\|_K)\,\mathrm{d}t \tag{37}$$

Remark 3.1

If ϕ_T is sufficiently regular we may use dual weights of the form $\omega_{\mathrm{T},K}=(k_n\|\dot{\phi}_\mathrm{T}\|_K+h_K^m \|D^m\phi_\mathrm{T}\|_K)$ with $m\geqslant 1$, thus obtaining a higher order on the factor h_K^m. However, for complicated flows, relying on less regularity of the dual problem may be a more robust alternative in practice.

3.3. Estimates of the modelling error

Starting from the definition of the modelling error (27) we obtain

$$m_\mathrm{F}(\mathbf{u}_\mathrm{F}-\mathbf{U}_\mathrm{F}) = a_\mathrm{T}(\mathbf{U}_\mathrm{F}; u_\mathrm{T}, \phi_\mathrm{T}) - a_\mathrm{T}(\mathbf{u}_\mathrm{F}; u_\mathrm{T}, \phi_\mathrm{T}) \tag{38}$$

$$= \int_I (u_\mathrm{T}, \mathbf{U}_\mathrm{F}\cdot\nabla\phi_\mathrm{T})\,\mathrm{d}t - \int_I (u_\mathrm{T}, \mathbf{u}_\mathrm{F}\cdot\nabla\phi_\mathrm{T})\,\mathrm{d}t \tag{39}$$

$$= -\int_I (u_\mathrm{T}\nabla\phi_\mathrm{T}, (\mathbf{u}_\mathrm{F}-\mathbf{U}_\mathrm{F}))\,\mathrm{d}t \tag{40}$$

which implies that

$$m_\mathrm{F}(\mathbf{v}) = -\int_I (u_\mathrm{T}\nabla\phi_\mathrm{T}, \mathbf{v})\,\mathrm{d}t \tag{41}$$

is the relevant goal functional for the fluid solver if we want to determine the original target quantity $m_\mathrm{T}(u_\mathrm{T})$ accurately.

To derive an error representation formula for $m_\mathrm{F}(\cdot)$ we introduce the following dual fluid flow problem: find $(\boldsymbol{\phi}_\mathrm{F},\theta)\in\mathbf{V}_\mathrm{F}$ such that

$$a_\mathrm{F}'((\mathbf{v},w),(\boldsymbol{\phi}_\mathrm{F},\theta)) = m_\mathrm{F}(\mathbf{v}) \quad \forall(\mathbf{v},w)\in\mathbf{V}_\mathrm{F} \tag{42}$$

where the bilinear form $a_\mathrm{F}'(\cdot,\cdot)$ is defined by

$$\begin{aligned} a_\mathrm{F}'((\mathbf{v},w),(\boldsymbol{\phi}_\mathrm{F},\theta)) = \int_I & (\dot{\mathbf{v}},\boldsymbol{\phi}_\mathrm{F}) + (\mathbf{u}_\mathrm{F}\cdot\nabla\mathbf{v},\boldsymbol{\phi}_\mathrm{F}) + (\mathbf{v}\cdot\nabla\mathbf{U}_\mathrm{F},\boldsymbol{\phi}_\mathrm{F}) + \nu(\nabla\mathbf{v},\nabla\boldsymbol{\phi}_\mathrm{F}) \\ & -\frac{1}{\rho}(\nabla\cdot\mathbf{v},\theta) - (w,\nabla\cdot\boldsymbol{\phi}_\mathrm{F})\,\mathrm{d}t \end{aligned} \tag{43}$$

Setting $\mathbf{v}=\mathbf{u}_\mathrm{F}-\mathbf{U}_\mathrm{F}$ and $w=p-P$ and using the definition of the dual problem (42) we obtain

$$m_\mathrm{F}(\mathbf{u}_\mathrm{F}-\mathbf{U}_\mathrm{F}) = a_\mathrm{F}'((\mathbf{u}_\mathrm{F}-\mathbf{U}_\mathrm{F}, p-P),(\boldsymbol{\phi}_\mathrm{F},\theta)) \tag{44}$$

$$= a_\mathrm{F}((\mathbf{u}_\mathrm{F},p),(\boldsymbol{\phi}_\mathrm{F},\theta)) - a_\mathrm{F}((\mathbf{U}_\mathrm{F},P),(\boldsymbol{\phi}_\mathrm{F},\theta)) \tag{45}$$

$$= 0 - a_\mathrm{F}((\mathbf{U}_\mathrm{F},P),(\boldsymbol{\phi}_\mathrm{F},\theta)) \tag{46}$$

$$= -a_\mathrm{F}((\mathbf{U}_\mathrm{F},P),(\boldsymbol{\phi}_\mathrm{F}-\pi\boldsymbol{\phi}_\mathrm{F},\theta-\pi\theta)) \tag{47}$$

where we have used the Galerkin orthogonality to subtract interpolants $(\pi\boldsymbol{\phi}_\mathrm{F},\pi\theta)\in\mathbf{W}_{\mathrm{F},h,n}$.

DOI: 10.1002/fld

Defining the weak residual $R_{\mathrm{F}}(\mathbf{U}_{\mathrm{F}}, P) \in \mathbf{V}_{\mathrm{F}}^*$ by

$$\langle R_{\mathrm{F}}(\mathbf{U}_{\mathrm{F}}, P), (\mathbf{v}, w)\rangle_{\Omega\times I} = -a_{\mathrm{F}}((\mathbf{U}_{\mathrm{F}}, P), (\mathbf{v}, w)) \quad \forall(\mathbf{v}, w)\in \mathbf{V}_{\mathrm{F}} \tag{48}$$

we obtain the following error representation formula:

$$m_{\mathrm{F}}(\mathbf{u}_{\mathrm{F}}-\mathbf{U}_{\mathrm{F}}) = \langle R_{\mathrm{F}}(\mathbf{U}_{\mathrm{F}}, P), (\boldsymbol{\phi}_{\mathrm{F}}-\pi\boldsymbol{\phi}_{\mathrm{F}}, \theta-\pi\theta)\rangle_{\Omega\times I} \tag{49}$$

This is just the discretization error resulting from the finite element method for the Navier–Stokes equations. Note that we do not get any modelling error terms, since we assume that the input to these equations are exact.

Breaking the discretization error (49) into a sum over the elements and estimating using the Cauchy–Schwartz inequality we obtain the following *a posteriori* error estimate:

$$m_{\mathrm{F}}(\mathbf{u}_{\mathrm{F}}-\mathbf{U}_{\mathrm{F}}) \leqslant \sum_{K\in\mathscr{K}} \boldsymbol{\rho}_{\mathrm{F},K}\cdot\boldsymbol{\omega}_{\mathrm{F},K} \tag{50}$$

where the time-averaged element indicators $\boldsymbol{\rho}_{\mathrm{F},K}$ and weights $\boldsymbol{\omega}_{\mathrm{F},K}$ are given by (see [7])

$$\boldsymbol{\rho}_{\mathrm{F},K} = \int_I (R_1 \quad R_2)\,\mathrm{d}t, \quad \boldsymbol{\omega}_{\mathrm{F},K} = \int_I (W_1 \quad W_2)\,\mathrm{d}t \tag{51}$$

where

$$R_1 = \|\mathbf{f}-\dot{\mathbf{U}}_{\mathrm{F}}-(\mathbf{U}_{\mathrm{F}}\cdot\nabla\mathbf{U}_{\mathrm{F}})+\nu\Delta\mathbf{U}_{\mathrm{F}}-\frac{1}{\rho}\nabla P\|_K+\frac{1}{2}h_K^{-1/2}\|\nu[\mathbf{n}\cdot\nabla\mathbf{U}_{\mathrm{F}}]\|_{\partial K\setminus\Gamma} \tag{52}$$

$$R_2 = \|\nabla\cdot\mathbf{U}_{\mathrm{F}}\|_K \tag{53}$$

$$W_1 = C_1(k_n\|\dot{\boldsymbol{\phi}}_{\mathrm{F}}\|_K+h_K\|\nabla\boldsymbol{\phi}_{\mathrm{F}}\|_K) \tag{54}$$

$$W_2 = C_2(k_n\|\dot{\boldsymbol{\theta}}\|_K+h_K\|\nabla\boldsymbol{\theta}\|_K) \tag{55}$$

Remark 3.2
The bilinear form $a'_{\mathrm{F}}(\cdot,\cdot)$ contains the exact velocity $\mathbf{u}_{\mathrm{F}}$ which, of course, is unknown. In practice, $\mathbf{u}_{\mathrm{F}}$ is therefore approximated by its computed counterpart $\mathbf{U}_{\mathrm{F}}$. Numerical experience indicates that this simplification generally works well.

Remark 3.3
The variational equation (42) corresponds to the following strong form of the linearized dual Navier–Stokes equations: find $\boldsymbol{\phi}_{\mathrm{F}}:\Omega\times I\to\mathbf{R}^3$ and $\theta:\Omega\times I\to\mathbf{R}$ such that

$$-\dot{\boldsymbol{\phi}}_{\mathrm{F}}-(\mathbf{u}_{\mathrm{F}}\cdot\nabla)\boldsymbol{\phi}_{\mathrm{F}}+\nabla\mathbf{U}_{\mathrm{F}}\cdot\boldsymbol{\phi}_{\mathrm{F}}-\nu\Delta\boldsymbol{\phi}_{\mathrm{F}}+\frac{1}{\rho}\nabla\theta=\boldsymbol{\Psi}, \quad (\mathbf{x},t)\in\Omega\times I \tag{56a}$$

$$\nabla\cdot\boldsymbol{\phi}_{\mathrm{F}}=0, \quad (\mathbf{x},t)\in\Omega\times I \tag{56b}$$

$$\boldsymbol{\phi}_{\mathrm{F}}=\mathbf{0}, \quad (\mathbf{x},t)\in\Gamma\setminus\Gamma_{\mathrm{out}} \tag{56c}$$

$$\nu\mathbf{n}\cdot\nabla\boldsymbol{\phi}_{\mathrm{F}}+\mathbf{n}\left(\mathbf{u}_{\mathrm{F}}\cdot\boldsymbol{\phi}_{\mathrm{F}}-\frac{1}{\rho}\theta\right)=\mathbf{0}, \quad (\mathbf{x},t)\in\Gamma_{\mathrm{out}} \tag{56d}$$

$$\boldsymbol{\phi}_{\mathrm{F}}(\cdot,\hat{T})=\mathbf{0}, \quad \mathbf{x}\in\Omega \tag{56e}$$

DOI: 10.1002/fld

where $(\nabla \mathbf{U}_{\mathrm{F}} \cdot \boldsymbol{\phi}_{\mathrm{F}})_j = (\partial_j \mathbf{U}_{\mathrm{F}}) \cdot \boldsymbol{\phi}_{\mathrm{F}}$, and $\boldsymbol{\Psi} = -u_{\mathrm{T}} \nabla \phi_{\mathrm{T}}$. Note that the dual problem is evolved backwards in time, starting from $t = \hat{T}$.

3.4. *A posteriori error estimate for the coupled problem*

Combining the error representation formula (28) for the original coupled problem with the individual *a posteriori* error estimates for the heat transfer (35) and fluid flow problems (50) we obtain the following *a posteriori* error estimate:

$$m_{\mathrm{T}}(u_{\mathrm{T}} - U_{\mathrm{T}}) \leqslant \sum_{K \in \mathscr{K}} \rho_{\mathrm{T},K} \omega_{\mathrm{T},K} + \boldsymbol{\rho}_{\mathrm{F},K} \cdot \boldsymbol{\omega}_{\mathrm{F},K} \tag{57}$$

$$\equiv \sum_{K \in \mathscr{K}} \eta_K \tag{58}$$

where we introduced the element indicator η_K. We note that the resulting *a posteriori* error estimate involves standard dual weighted residual contributions from the heat transfer and the fluid flow problems, where the particular weights account for the propagation of an error from the fluid flow problem to the heat transfer problem. As previously mentioned, the *a posteriori* error analysis for nonlinear equations is not as straightforward as for linear ones, and the error bounds are in general not mathematically rigorous due to the linearization of the dual problems.

3.5. *Adaptive algorithm*

Starting from the *a posteriori* error estimate (57) a basic adaptive algorithm takes the form:

Algorithm 1

1. Solve the primal problems, starting with the Navier–Stokes equations (1) to obtain the fluid velocity $\mathbf{u}_{\mathrm{F}}$, and then solve the heat equation (2) with $\mathbf{u}_{\mathrm{F}}$ as an advection field for the temperature u_{T}.
2. Solve the dual heat transfer problem (20), using the specified goal functional $m_{\mathrm{T}}(\cdot)$ as right-hand side, for the dual temperature ϕ_{T}.
3. Use ϕ_{T} to compute the modelling functional $m_{\mathrm{F}}(\cdot)$, defined by (41), and solve the dual linearized Navier–Stokes equations (56) for the dual velocity $\boldsymbol{\phi}_{\mathrm{F}}$ and pressure θ.
4. Compute the error indicators η_K and use them together with a refinement criterion to select elements that contribute the most to the error. Refine the selected elements.
5. Repeat steps 1–4 until satisfactory results have been obtained.

Note that each loop of Algorithm 1 involves two inner timeloops. First, the primal equations must be solved from $t = 0$ to $t = \hat{T}$, and then the dual equations must be solved from $t = \hat{T}$ to $t = 0$, that is, the primal equations must be solved and their solutions stored before we can start solving the dual equations. This is computationally expensive, but might still be a faster way of obtaining accurate values of the goal functional than to solve the primal equations on uniformly refined meshes.

Remark 3.4

We use the common refinement criterion: refine all elements K such that

$$\eta_K \geqslant \alpha \max_{K \in \mathscr{K}} \eta_K \tag{59}$$

where $0 \leqslant \alpha < 1$ is a user-defined parameter.

3.6. A special goal functional: time-integrated heat flux

Let us assume that the desired goal quantity is the time-integrated flux,

$$\int_I (-\varepsilon \mathbf{n} \cdot \nabla u_{\mathrm{T}}, 1)_{\Gamma_{\mathrm{goal}}} \, \mathrm{d}t \tag{60}$$

through one of the hot boxes with boundary Γ_{goal}. To compute this, given the discrete solution U_{T} we note that Green's formula gives

$$(\varepsilon \mathbf{n} \cdot \nabla u_{\mathrm{T}}, v)_{\Gamma} = (\dot{u}_{\mathrm{T}} + \nabla \cdot (\mathbf{U}_{\mathrm{F}} u_{\mathrm{T}}), v) + (\varepsilon \nabla u_{\mathrm{T}}, \nabla v) \tag{61}$$

$$= (-\kappa(u_{\mathrm{T}} - g), v)_{\Gamma} \tag{62}$$

where we used the variational formulation (9a) and the boundary conditions for $\mathbf{U}_{\mathrm{F}}$. Although these three expressions are equivalent for the exact solution u_{T} they are not for the discrete solution U_{T}. Using (61) to compute the numerical heat flux avoids evaluating the normal derivative of U_{T}, and also results in a higher rate of convergence [12]. We therefore define the affine functional

$$\tilde{m}_{\mathrm{T}}(U_{\mathrm{T}}) = \int_I (\kappa(U_{\mathrm{T}} - g), \Psi)_{\Gamma} \, \mathrm{d}t \tag{63}$$

where $\Psi = 1$ on Γ_{goal} and $\Psi = 0$ on $\Gamma \setminus \Gamma_{\mathrm{goal}}$. Using this definition we obtain the following error representation formula:

$$\tilde{m}_{\mathrm{T}}(u_{\mathrm{T}}) - \tilde{m}_{\mathrm{T}}(U_{\mathrm{T}}) = \int_I (\kappa(u_{\mathrm{T}} - g), \Psi)_{\Gamma} \, \mathrm{d}t - \int_I (\kappa(U_{\mathrm{T}} - g), \Psi)_{\Gamma} \, \mathrm{d}t \tag{64}$$

$$= \int_I (\kappa \Psi, u_{\mathrm{T}} - U_{\mathrm{T}})_{\Gamma} \, \mathrm{d}t \tag{65}$$

$$\equiv m_{\mathrm{T}}(u_{\mathrm{T}} - U_{\mathrm{T}}) \tag{66}$$

where our goal functional $m_{\mathrm{T}}(\cdot)$ was introduced. Using (66) as the right-hand side in (20) gives

$$m_{\mathrm{T}}(v) = \int_I (\dot{v}, \phi) - (v, \mathbf{U}_{\mathrm{F}} \cdot \nabla \phi) + (\varepsilon \nabla v, \nabla \phi) + (\kappa v, \phi)_{\Gamma} \, \mathrm{d}t \tag{67}$$

This variational dual heat transfer problem is equivalent to the following strong form: find the dual temperature $\phi_{\mathrm{T}} : \Omega \times I \to \mathbf{R}$ such that

$$-\dot{\phi}_{\mathrm{T}} - \mathbf{U}_{\mathrm{F}} \cdot \nabla \phi_{\mathrm{T}} - \nabla \cdot (\varepsilon \nabla \phi_{\mathrm{T}}) = 0, \quad (\mathbf{x}, t) \in \Omega \times I \tag{68a}$$

$$\phi_{\mathrm{T}} = 0, \quad (\mathbf{x}, t) \in \Gamma \setminus (\Gamma_{\mathrm{box}} \cup \Gamma_{\mathrm{out}}) \times I \tag{68b}$$

$$-\mathbf{n} \cdot \varepsilon \nabla \phi_{\mathrm{T}} = \kappa(\phi_{\mathrm{T}} - \Psi), \quad (\mathbf{x}, t) \in \Gamma_{\mathrm{goal}} \times I \tag{68c}$$

$$-\mathbf{n} \cdot \varepsilon \nabla \phi_{\mathrm{T}} = \kappa \phi_{\mathrm{T}}, \quad (\mathbf{x}, t) \in \Gamma_{\mathrm{box}} \setminus \Gamma_{\mathrm{goal}} \times I \tag{68d}$$

DOI: 10.1002/fld

$$\mathbf{n}\cdot\varepsilon\nabla\phi_{\mathrm{T}}=0, \quad (\mathbf{x},t)\in\Gamma_{\mathrm{out}}\times I \tag{68e}$$

$$\phi_{\mathrm{T}}(\cdot,\hat{T})=0, \quad \mathbf{x}\in\Omega \tag{68f}$$

Remark 3.5

The dual problems are solved only once, and then backwards over the entire time interval I from $t=\hat{T}$ to $t=0$, for each adaptive mesh refinement loop. This procedure works since $m_{\mathrm{T}}(\cdot)$ is a linear functional acting on functions defined on the space–time domain V_{T}, that is, $m_{\mathrm{T}}(u_{\mathrm{T}})$ is a quantity weighted in both time and space of the form $m_{\mathrm{T}}(u_{\mathrm{T}})=\int_I(u_{\mathrm{T}},\psi)\,\mathrm{d}t$ with weight ψ. In contrast, had we been interested in, for instance, a functional of the form $m_{\mathrm{T}}(u_{\mathrm{T}})=\max_{\mathrm{T}\in I}(u_{\mathrm{T}},\psi)$, then it would have been necessary to solve a dual problem starting at the end of each time step and then consider the maximum of all the errors on I. Of course, this would be computationally very expensive.

4. NUMERICAL EXAMPLES

In this section we illustrate the error estimation methodology of Algorithm 1. The goal of the computation is the accurate computation of the heat flux out of a hot box, as defined by the goal functional $m_{\mathrm{T}}(\cdot)$. We study the performance of the algorithm by looking at the spatial adaptation of the mesh and aim at obtaining a good distribution of nodes for this particular target quantity. However, we do not consider the temporal adaptation of the mesh.

4.1. Setup

4.1.1. Geometric specifications. The outer dimensions of the channel Ω_0 are $\Omega_0=\{\mathbf{x}:0\leqslant x\leqslant 12, 0\leqslant y\leqslant 4, 0\leqslant z\leqslant 4\}$. The inflow and outflow regions are given by $\Gamma_{\mathrm{in}}=\{\mathbf{x}:x=0, 0\leqslant y\leqslant 4, 3\leqslant z\leqslant 4\}$, and $\Gamma_{\mathrm{out}}=\{\mathbf{x}:x=12, 0\leqslant y\leqslant 4, 0\leqslant z\leqslant 1\}$ (see Figure 1). We shall present numerical results for two different geometries. In the first case, we study a single hot box B with dimensions

$$B=\{\mathbf{x}:6\leqslant x\leqslant 7.5, 1.5\leqslant y\leqslant 2.5, 1.5\leqslant z\leqslant 2.5\} \tag{69}$$

In the second case, we have two boxes

$$B_1=\{\mathbf{x}:8.25\leqslant x\leqslant 9.75, 1.5\leqslant y\leqslant 2.5, 2\leqslant z\leqslant 3\} \tag{70}$$

$$B_2=\{\mathbf{x}:4.5\leqslant x\leqslant 6, 1.5\leqslant y\leqslant 2.5, 1\leqslant z\leqslant 2\} \tag{71}$$

The computational domain is thus either $\Omega=\Omega_0\setminus B$ or $\Omega=\Omega_0\setminus(B_1\cup B_2)$.

4.1.2. Parameter settings and boundary conditions. The parameters for the Navier–Stokes equations (1) are $v=0.01$ and $\rho=1$. The low value of the viscosity v means that we have a Reynolds number of order 10^2 (since the typical velocity and length scale are 1). The velocity inflow profile is $\mathbf{v}_{\mathrm{in}}=y(y-4)(z-3)(z-4)$.

For the heat equation (2) $\varepsilon=0.01$, $\kappa=g=1$ on Γ_{box}, $\kappa=0$ on Γ_{out}, and $\kappa=10^6$ on the rest of the boundary Γ.

In all simulations, the number of time steps were 4000 with a uniform time step of $k=k_n=0.005$.

4.2. *Numerical methods*

4.2.1. Navier–Stokes equations. The finite element method (1) gives rise to the following Crank–Nicolson-type time-stepping scheme

$$\begin{bmatrix} \frac{1}{k}\mathbf{M}+\frac{1}{2}(\nu\mathbf{A}+\mathbf{N}) & \mathbf{B}^{\mathrm{T}} \\ \mathbf{B} & \mathbf{0} \end{bmatrix} \begin{bmatrix} \mathbf{U}_{\mathrm{F}}^{n} \\ \mathbf{P}^{n-1/2} \end{bmatrix} = \begin{bmatrix} \left(\frac{1}{k}\mathbf{M}-\frac{1}{2}(\nu\mathbf{A}+\mathbf{N})\right)\mathbf{U}_{\mathrm{F}}^{n-1} \\ \mathbf{0} \end{bmatrix} \tag{72}$$

where the matrices involved correspond to differential operators as follows, $\mathbf{M}\sim Id$, $\mathbf{A}\sim -\mathrm{diag}\,\Delta$, $\mathbf{N}\sim\mathbf{u}_{\mathrm{F}}\cdot\nabla$, $\mathbf{B}\sim\nabla\cdot$, and $\mathbf{B}^{\mathrm{T}}\sim\nabla$, and where $\mathbf{U}_{\mathrm{F}}^{n}$ denotes a vector of nodal values of $\mathbf{U}_{\mathrm{F}}$ at time t_n, $n=1,\ldots,N$, and similarly for the pressure $\mathbf{P}$.

The matrix elements $M_{ij}, A_{ij},\ldots,$ are evaluated for standard trilinear shape functions on a hexahedral mesh of the domain Ω. The mesh can be locally refined by splitting each hexahedron into eight similar subhexahedra. When two hexahedra of different sizes meet, we use the constrained hanging node technique (cf. [8]) to preserve the continuity of the finite element functions. A restriction is made on the mesh that no neighboring elements can differ more than one level of subdivision.

To cope with convection-dominated flows we have added a streamline–diffusion [24]-type term $\delta\mathbf{N}\mathbf{N}^{\mathrm{T}}$, where δ is a stabilization parameter, to the matrix $\nu\mathbf{A}+\mathbf{N}$. However, when running the simulations presented in this paper we have not found it necessary to use this stabilization.

In order to solve the linear system (72) we have used an inexact matrix factorization technique. The main idea is to replace the global coefficient matrix with its incomplete block LU-factorization. In doing so, (72) can be approximately solved by performing the following three steps:

1.
$$\left(\frac{1}{k}\mathbf{M}+\frac{1}{2}(\nu\mathbf{A}+\mathbf{N})\right)\tilde{\mathbf{U}}_{\mathrm{F}}^{n}=\left(\frac{1}{k}\mathbf{M}-\frac{1}{2}(\nu\mathbf{A}+\mathbf{N})\right)\mathbf{U}_{\mathrm{F}}^{n-1} \tag{73}$$

2.
$$\mathbf{B}\mathbf{M}^{-1}\mathbf{B}^{\mathrm{T}}\mathbf{P}^{n-1/2}=\frac{1}{k}\mathbf{B}\tilde{\mathbf{U}}_{\mathrm{F}}^{n} \tag{74}$$

3.
$$\mathbf{U}_{\mathrm{F}}^{n}=\tilde{\mathbf{U}}_{\mathrm{F}}^{n}-k\mathbf{M}^{-1}\mathbf{B}\mathbf{P}^{n-1/2} \tag{75}$$

This is a discrete Chorin-type method involving a pressure Poisson equation (74), which introduces a certain amount of stabilization into the scheme. In particular, this stabilization allows for the use of equal-order interpolation spaces $\mathbf{V}_h$ and Q_h for the velocity and pressure, respectively (see [5]).

4.2.2. The heat equation. Similar to the Navier–Stokes equations, the prototype finite element method (19) yields the following Crank–Nicolson time-stepping scheme for the heat equation

$$\left(\frac{1}{k}\mathbf{M}+\frac{1}{2}\mathbf{A}\right)\mathbf{U}_{\mathrm{T}}^{n}=\left(\frac{1}{k}\mathbf{M}-\frac{1}{2}\mathbf{A}\right)\mathbf{U}_{\mathrm{T}}^{n-1}+\mathbf{G} \tag{76}$$

DOI: 10.1002/fld

where $\mathbf{M}\sim Id$, $\mathbf{A}\sim-\Delta$, and $\mathbf{G}$ represents the load vector arising from the boundary conditions. To be able to handle advection-dominated heat flows we have also here added a streamline–diffusion term to $\mathbf{A}$.

Needless to say, when calculating the indicators η_K, we approximate the continuous duals ϕ_{F}, θ, and ϕ_{T} with their discrete counterparts $\mathbf{\Phi}_{\mathrm{F}}$, Θ and Φ_{T}, which are solved with the same numerical methods as the primal problems and on the same meshes.

Finally, we mention that to save computer time and memory we store the velocity $\mathbf{U}_{\mathrm{F}}$ needed for the linearized Navier–Stokes dual only for every 40th time step (i.e. the discrete dual equation is only reassembled every 40th time step).

4.3. Example 1—one hot box

We consider a case with one interior hot box B, and the time-integrated flux goal functional (66) with $\Gamma_{\mathrm{goal}}=\Gamma_{\mathrm{box}}$. The problem is solved using the adaptive procedure of Algorithm 1 with a mesh refinement strategy using $\alpha=0.1$. After four refinements we obtain the mesh shown in Figure 3.

In Figure 4 we show a series of cross-sectional images of the temperature isocontours around the box. Streamlines of the velocity field is displayed in Figure 5 showing the evolution of the flow pattern of the advection field.

From Figure 3 it can be clearly seen that the mesh refinement is localized to the vicinity of the box, as can be expected if the heat flux out of the box is the quantity of interest. To study the convergence of this target quantity we used a ‘truth-grid solution’ as a reference value, that is, the time-integrated flux obtained from a computation on a big uniform mesh with roughly 3×10^5 elements with additional layers of refinement around the box (see Figure 6). After 15 refinements, using $\alpha=0.65$, we obtained the convergence plot of Figure 7, which shows the relative error (compared with the reference value) *versus* the number of elements (DOFs). Using a simple linear regression we find the convergence rate to be close to 4. The obtained value of the time-integrated heat flux computed on the ‘truth-grid’ was -1.16×10^3.

In Table I we show the accumulated computational time after a given number of adaptive refinement loops compared with the time required to solve only the primal equations on the ‘truth-grid’. These results clearly illustrate the advantage of an adaptive mesh refinement, since sufficient accuracy of the goal quantity is obtained with considerably reduced computational time.

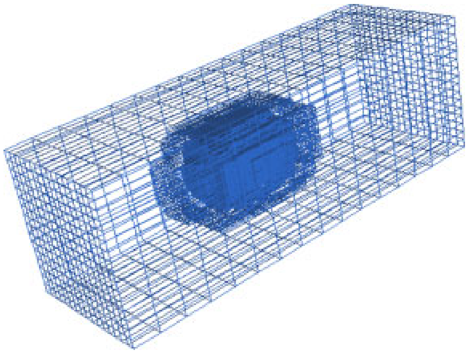

Figure 3. Refined mesh with one hot box after four mesh refinements.

DOI: 10.1002/fld

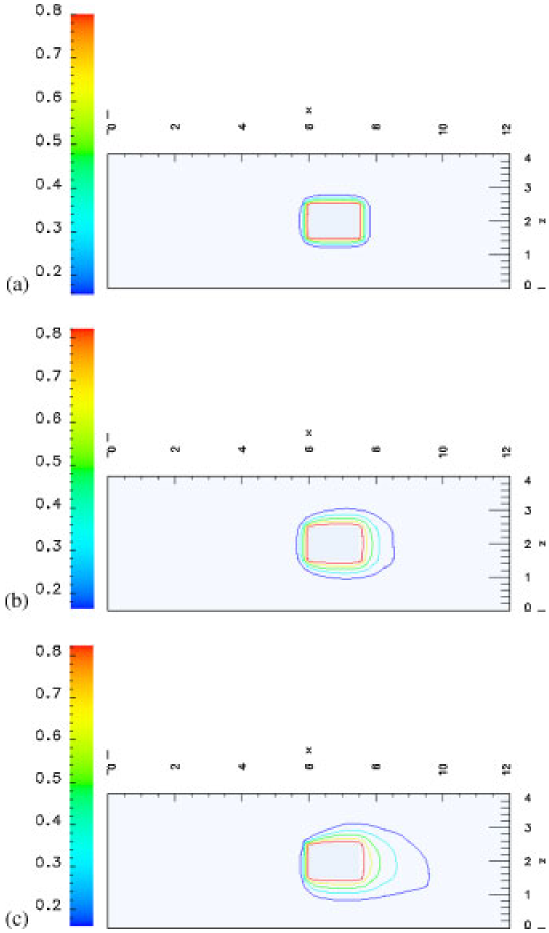

Figure 4. Isocontours of the temperature within the plane $y=2$ at three different time steps n: (a) $n=400$; (b) $n=2000$; and (c) $n=4000$.

4.4. *Example 2—two hot boxes*

In our next numerical example we study a case with two hot boxes B_1 and B_2 located within the channel, see Figure 1. The parameter settings and initial conditions are the same as for the previous case with one hot box. As before, the target quantity is the time-integrated heat flux out of one of the two boxes.

In Figure 8, we show the resulting meshes when either B_1 or B_2 is used as target box. As expected, the mesh refinement is made almost solely around the target box. However, more refinements are made around B_2 when B_1 is the target box than *vice versa*. This is explained by the fact that the upstream box B_2 influences the flow around the downstream box B_1, and it is therefore important to resolve both the region around B_2 and the region around B_1. The evolution of temperature and streamlines of the advection field are shown in Figures 9 and 10 (with B_2 as target box).

To try to understand the mesh refinement process we study the element residuals ρ_K shown in Figure 11. Recall that these are one half of the element indicators $\eta_K=\rho_K\omega_K$ (the other half

DOI: 10.1002/fld

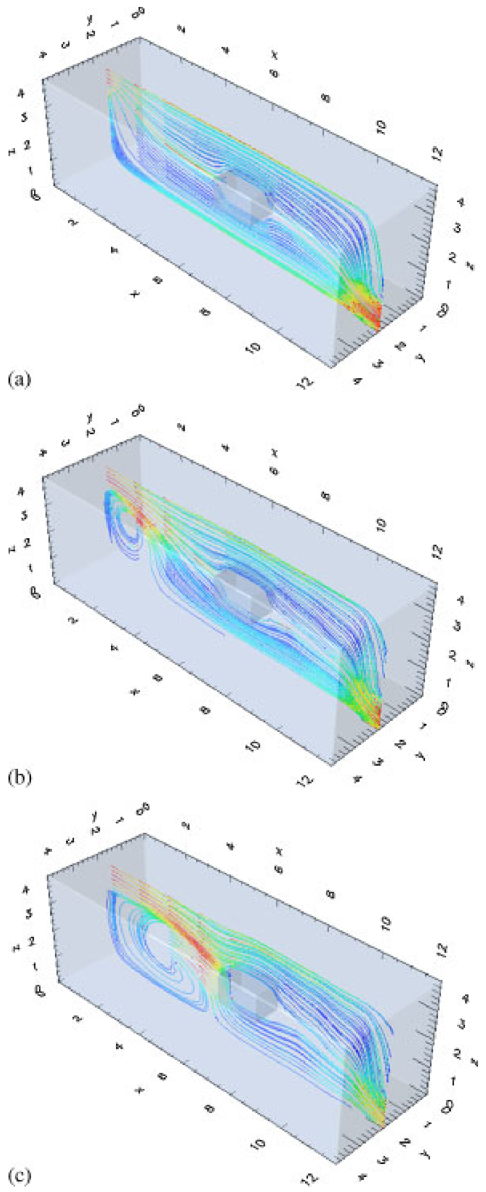

Figure 5. Streamlines of the velocity field seeded within the plane $y=2$ at three different time steps n. Note how the box divides the flow into two separate swirls: (a) $n=400$; (b) $n=2000$; and (c) $n=4000$.

being the dual weights ω_K), which are used to select elements to be refined. From Figure 11 it seems that the residuals are big around the boxes and near the inflow and outflow. This is natural since we can expect the solutions to have large gradients in these regions, and, consequently, one might expect to see mesh refinement there. The reason why no refinements have been made

DOI: 10.1002/fld

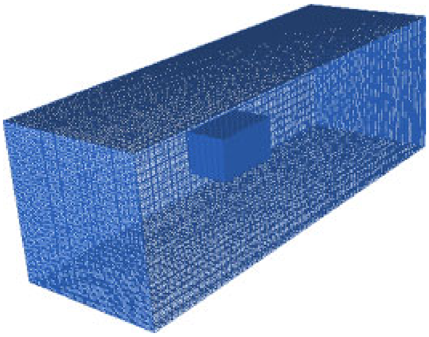

Figure 6. The ‘truth-grid’.

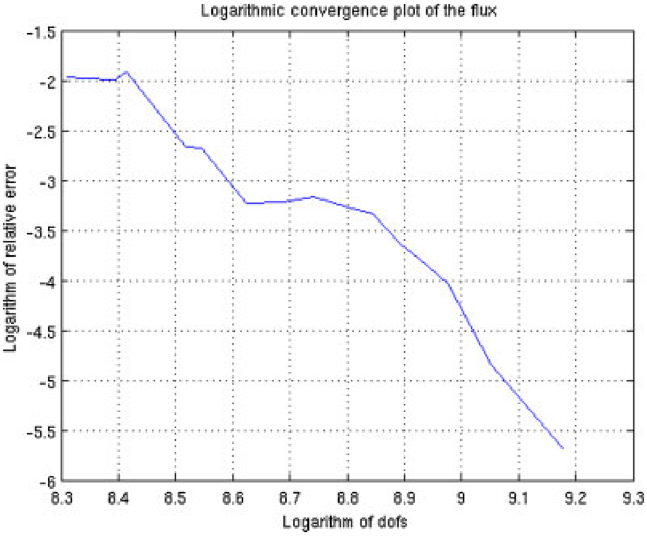

Figure 7. Comparison between the target quantity and a reference value that has been calculated on a ‘truth-grid’.

Table I. Computational time *versus* the number of mesh refinements compared to the computational time required to solve only the primal problem on the ‘truth-grid’.

Refinements	CPU time (h)
1	1
5	5
10	12
15	20
‘Truth-grid’	75

DOI: 10.1002/fld

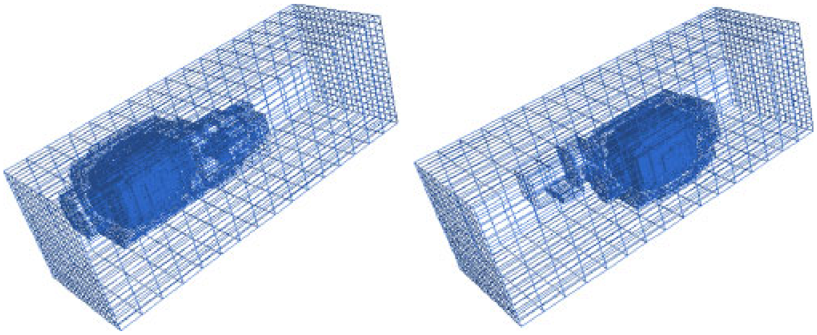

Figure 8. Refined meshes with two interior boxes and with $\Gamma_{B_1}=\Gamma_{\text{goal}}$ (left) and $\Gamma_{B_2}=\Gamma_{\text{goal}}$ (right).

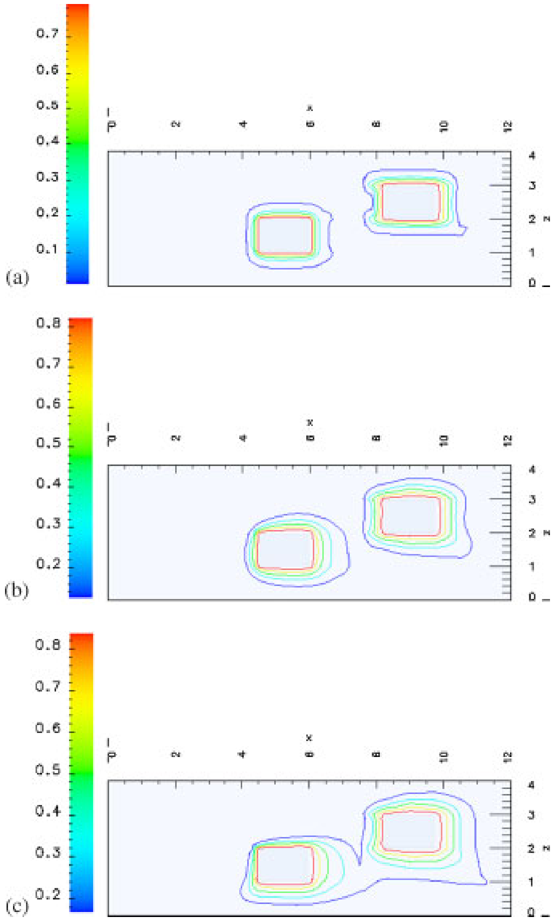

Figure 9. Isocontours of the temperature within the plane $y=2$ at three different time steps n, and with $\Gamma_{B_2}=\Gamma_{\text{goal}}$: (a) $n=400$; (b) $n=2000$; and (c) $n=4000$.

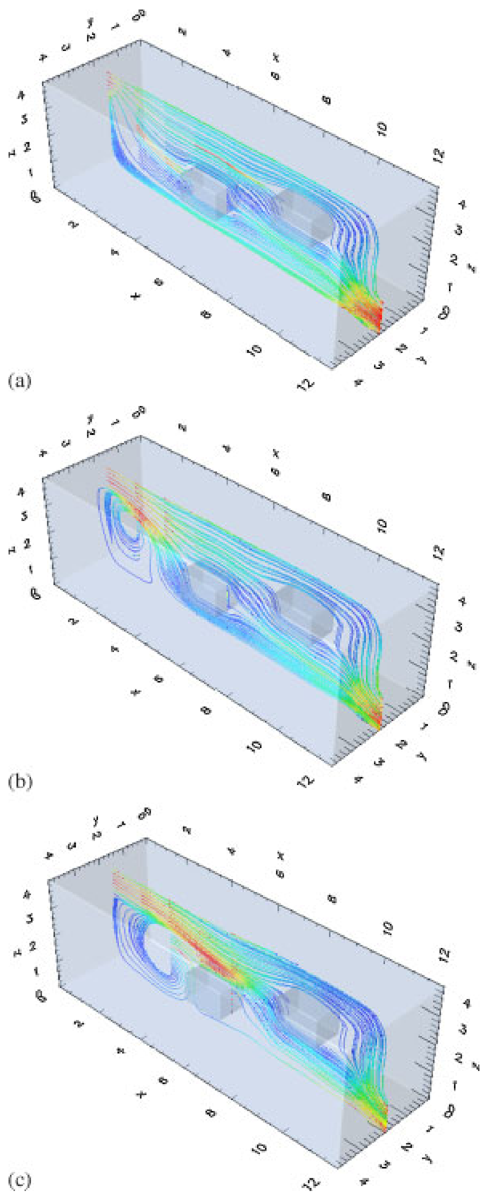

Figure 10. Streamlines of the velocity field seeded within the plane $y=2$ at three different time steps n, and with $\Gamma_{B_2}=\Gamma_{\text{goal}}$: (a) $n=400$; (b) $n=2000$; and (c) $n=4000$.

except around the boxes can be understood by looking at the dual solutions. In Figures 12–14 we show the evolution of the dual temperature. From these figures it is obvious that the only regions important to resolve to accurately determine the heat flux lies around the boxes. Thus, since the dual solutions are localized to the boxes, and especially to the target box, the dual weights will

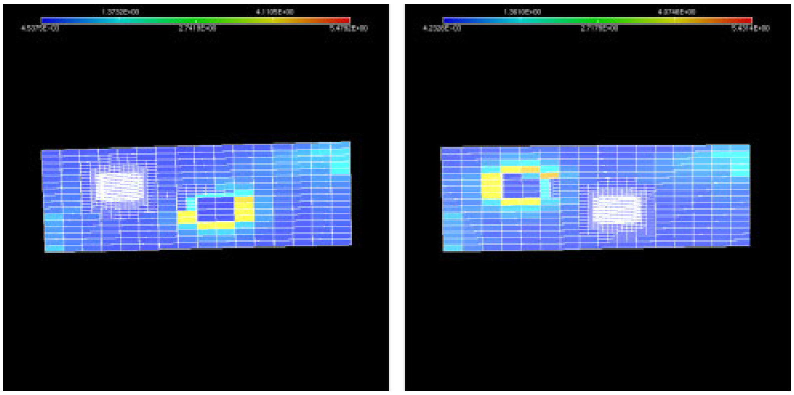

Figure 11. Element residuals on the refined mesh. Around the box, were refinements have been made, the residuals are close to zero, but close to the other box, were almost no refinements have been made, the residuals are large.

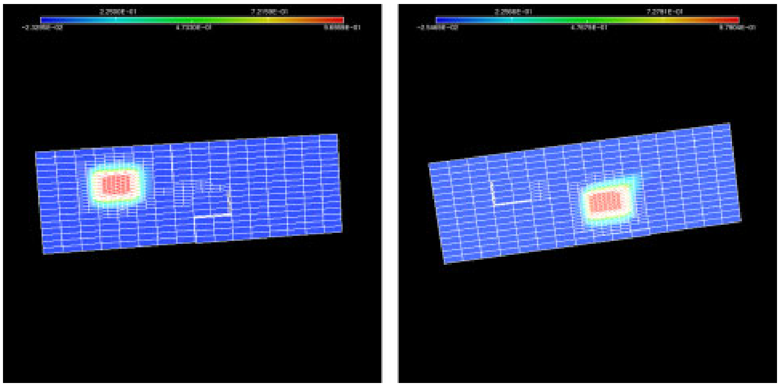

Figure 12. Dual temperatures after 40 time steps. The dual solutions, which are being weighted with the residuals in order to obtain the refinement indicators, are clearly localized around the target box.

contribute to the element indicators only there. Hence, the dual information pinpoints the important regions for computing the target quantity, and as a consequence valuable computational resources can be saved by concentrating the computational efforts to these regions.

5. CONCLUSIONS

We have presented an *a posteriori* error estimation framework for a one-way-coupled system describing heat transport in time-dependent incompressible fluid flow, together with adaptive algorithms for automatic construction of meshes tailored for the computation of specific goal functionals. The *a posteriori* error estimates account for the goal functional as well as the coupling between the equations and identifies in what sense the flow field must be accurate in order to

DOI: 10.1002/fld

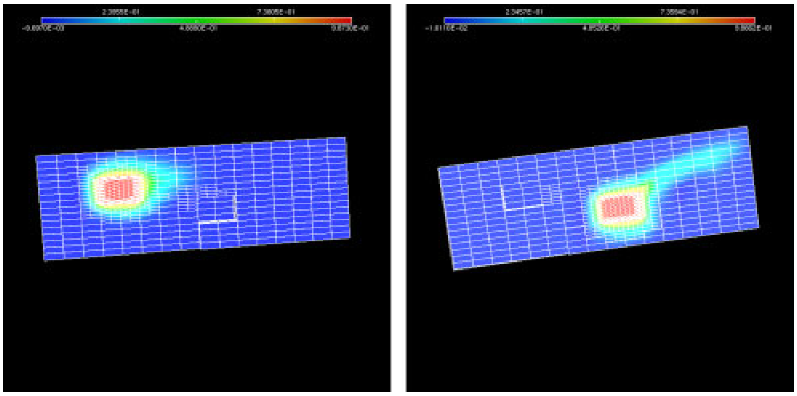

Figure 13. Dual temperatures after 2000 time steps. Note the lightly shaded areas that are important to resolve in order to accurately determine the heat flux.

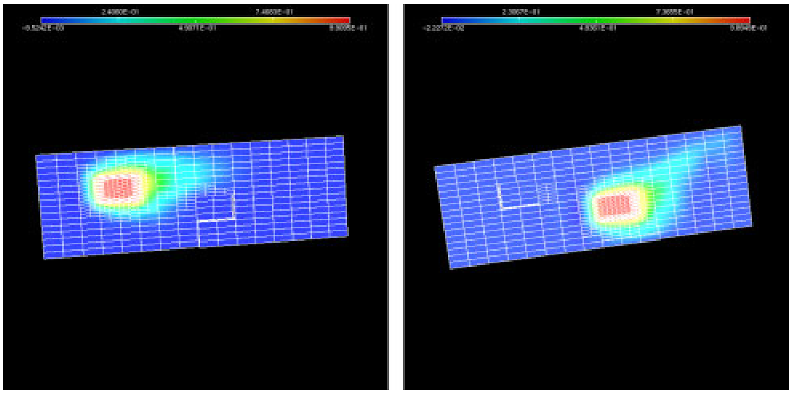

Figure 14. Dual temperatures after 4000 time steps. Note the difference from Figure 12, which implies that at the end of the simulation, only the flow very close to the box is important to accurately compute, whereas in the beginning the flow near the inflow is also of importance.

obtain accuracy in the goal functional. The approach is demonstrated on a three-dimensional test case involving non-stationary flow in a channel with immersed boxes. The goal quantity is the integrated heat flow through the boundary of one of the boxes. It is shown that the adaptive algorithm identifies areas where increased mesh resolution is needed, typically in the vicinity of the box of interest but also in upstream areas that influence the flow around the box of interest. We emphasize that these results are obtained automatically without any user interaction other than specification of the box of interest. We conclude that our results indicate that duality-based adaptive algorithms may be useful also in more complex fluids applications where it may be difficult and time consuming to design a suitable mesh given a computational goal. In future work we plan on addressing heat-driven flow, which is modelled by a two-way coupled system and also test the method in more complex examples.

DOI: 10.1002/fld

REFERENCES

1. Larson MG, Bengzon F. Adaptive finite element approximation of multiphysics problems. *Communications in Numerical Methods in Engineering* 2007; DOI: 10.1002/cnm.1087.
2. Larson MG, Målqvist A. Goal oriented adaptivity for coupled flow and transport problems with applications in oil reservoir simulations. *Computer Methods in Applied Mechanics and Engineering* 2007; **196**(37–40):3546–3561.
3. Carey V, Estep D, Tavener S. A posteriori analysis and adaptive error control for operator decomposition methods for coupled elliptic systems. I: one way coupled systems. *SIAM Journal on Numerical Analysis* 2006; in revision.
4. Carey V, Estep D, Tavener S. A posteriori analysis and adaptive error control for operator decomposition methods for elliptic systems II: fully coupled systems. 2007; in preparation.
5. Guermond JL, Minev P, Shen J. An overview of projection methods for incompressible flows. *Computer Methods in Applied Mechanics and Engineering* 2006; **195**(44–47):6011–6045.
6. Becker R, Heuveline V, Rannacher R. An optimal control approach to adaptivity in computational fluid mechanics. *International Journal for Numerical Methods in Fluids* 2002; **40**(1–2):105–120 (*ICFD Conference on Numerical Methods for Fluid Dynamics*, Oxford, 2001).
7. Hoffman J, Johnson C. *Computational Turbulent Incompressible Flow*. Applied Mathematics: Body and Soul, vol. 4. Springer: Berlin, 2007.
8. Bangerth W, Rannacher R. *Adaptive Finite Element Methods for Differential Equations*. Lectures in Mathematics ETH Zürich. Birkhäuser Verlag: Basel, 2003.
9. Eriksson K, Estep D, Hansbo P, Johnson C. Introduction to adaptive methods for differential equations. *Acta Numerica* 1995; **4**:105–158.
10. Estep DJ, Larson MG, Williams RD. Estimating the error of numerical solutions of systems of reaction–diffusion equations. *Memoirs of the American Mathematical Society* 2000; **146**(696):viii+109.
11. Carey GF. *Computational Grids*: *Generation*, *Adaptation*, *and Solution Strategies*. Series in Computational and Physical Processes in Mechanics and Thermal Sciences. Taylor & Francis: Washington, DC, 1997.
12. Giles MB, Larson MG, Levenstam J, Suli E. Adaptive error control for finite element approximations of the lift and drag in viscous flow. *Technical Report*, *NA97/06*, Oxford University Computing Laboratory, 1997.
13. Carey GF, Chow S-S, Seager MK. Approximate boundary-flux calculations. *Computer Methods in Applied Mechanics and Engineering* 1985; **50**(2):107–120.
14. Hughes TJR, Engel G, Mazzei L, Larson MG. The continuous Galerkin method is locally conservative. *Journal of Computational Physics* 2000; **163**(2):467–488.
15. Wildey T, Tavener S, Estep D. A posteriori error estimation of approximate boundary fluxes. *Communications in Numerical Methods in Engineering* 2006; DOI: 10.1002/cnm.1014.
16. Tritton DJ. *Physical Fluid Dynamics* (2nd edn). Oxford Science Publications, The Clarendon Press/Oxford University Press: New York, 1988.
17. Rannacher R. Finite element methods for the incompressible Navier–Stokes equations. *Fundamental Directions in Mathematical Fluid Mechanics*. Advances in Mathematical Fluid Mechanics. Birkhäuser: Basel, 2000; 191–293.
18. Chandrasekhar S. *Hydrodynamic and Hydromagnetic Stability*. The International Series of Monographs on Physics. Clarendon Press: Oxford, 1961.
19. Larson MG, Söderlund R. Adaptive finite element approximation of two way coupled problems. *Research Report in Mathematics No. 10*, Umeå University, 2007. ISBN: 978-91-7264-482-3, ISSN: 1653-0810.
20. Brenner SC, Scott LR. *The Mathematical Theory of Finite Element Methods* (2nd edn). Texts in Applied Mathematics, vol. 15. Springer: New York, 2002.
21. Scott LR, Zhang S. Finite element interpolation of nonsmooth functions satisfying boundary conditions. *Mathematics of Computation* 1990; **54**(190):483–493.
22. Tezduyar TE. *Stabilized Finite Element Formulations for Incompressible Flow Computations*. Advances in Applied Mechanics, vol. 28. Academic Press: Boston, MA, 1992; 1–44.
23. Thomée V. *Galerkin Finite Element Methods for Parabolic Problems* (2nd edn). Springer Series in Computational Mathematics, vol. 25. Springer: Berlin, 2006.
24. Johnson C. *Numerical Solution of Partial Differential Equations by the Finite Element Method*. Cambridge University Press: Cambridge, 1987.